Electronic Supplementary Information

(19 pages)

Solid-state chiral resolution mediated by stoichiometry: crystallizing etiracetam with $ZnCl_2$

Oleksii Shemchuk,[a)] Lixing Song,[b)] Koen Robeyns,[b)] Dario Braga,[a)] Fabrizia Grepioni*,[a)] and Tom Leyssens* [b)]

[a] Dipartimento di Chimica “Giacomo Ciamician”, Università di Bologna, Via Selmi, 2 – 40126 Bologna – Italy.

[b] Institute of Condensed Matter and Nanosciences, Université Catholique de Louvain, 1 Place Louis Pasteur, B-1348 Louvain-La-Neuve, Belgium

Table of Contents

***Please note that** in order to avoid possible confusion for the reader, in the present article we use the abbreviations RS-ETI to indicate etiracetam in its racemic form, S-ETI to indicate the active S-enantiomer (i.e. levetiracetam) and R-ETI to indicate the inactive R-enantiomer.*

---

1. Experimental Procedures

S-2-(2-oxopyrrolidin-1-yl)butanamide (Levetiracetam, *S*-ETI) was purchased from Xiamen Top Health Biochem Tech. Co., Ltd. (RS)-2-(2-oxopyrrolidin-1-yl)butanamide (Etiracetam, *RS*-ETI) was prepared by racemization of S-2-(2-oxopyrrolidin-1-yl)butanamide. 10g of S-2-(2-oxopyrrolidin-1-yl)butanamide together with catalytic amount (0.05 eq.) of MeONa were added to 10 mL of MeOH. The solution was kept at reflux under continuous stirring for 24h, and then cooled to room temperature. The compound crystallizes spontaneously. After filtration, the compound was washed twice with MeOH. The recovered compound was used as such. All the other reagents were purchased from Sigma and used without further purification.

1.1 Solution Synthesis. Equimolar quantities of the starting materials (*S*-ETI:$ZnCl_2$ 1:1 and *RS*-etiracetam:$ZnCl_2$ 2:1) were dissolved in 2 mL of ethanol at room temperature. Slow evaporation of the solvent at room temperature resulted in the formation of an oil-like substance, which after several days precipitated as complexes *S*-ETI·$ZnCl_2$ and *RS*-ETI_2·$ZnCl_2$.

1.2 Solid-state synthesis. Pure complexes of *S*-ETI·$ZnCl_2$ and *RS*-ETI_2·$ZnCl_2$ were obtained mechanochemically by ball-milling the stoichiometric ratios of the starting materials in an agate jar for 60 min in a Retsch MM200 ball miller, operated at a frequency of 25 Hz, with the addition of a drop of ethanol.

1.3 Slurry synthesis. *S*-ETI·$ZnCl_2$ and *RS*-ETI_2·$ZnCl_2$ were also obtained by slurrying for 2 days, in the minimum quantity of ethanol, methanol or water, the starting materials in the appropriate stoichiometric ratio.

1.4 Thermogravimetric analysis. TG analyses for *S*-ETI·$ZnCl_2$ and *RS*-ETI_2·$ZnCl_2$ were performed with a TGA/SDTA 851 Mettler Toledo instrument. Samples were placed in open aluminium oxide crucibles annealed at 1100 °C. The heating rate was 2 °C/min over the range 25-350 °C. All experiments were carried out under nitrogen atmosphere.

TGA measurements for *RS*-ETI, *S*-ETI and *R*-ETI·$ZnCl_2$ / *S*-ETI·$ZnCl_2$ conglomerates were performed with a PerkinElmer TGA7 in the temperature range 40-500 ºC under N_2 gas flow at a heating rate of 5.00 ºC min^{-1}.

1.5 Differential Scanning Calorimetry. DSC measurements for *S*-ETI·$ZnCl_2$ and *RS*-ETI_2·$ZnCl_2$ were performed on a TA DSC2500 with T0 technology, after calibration with indium. Samples were placed in aluminium perforated T0 pans, under continuous nitrogen flow. A heating ramp at 5°C/min from 30°C to 250°C was applied for all samples.

DSC thermograms for *RS*-ETI, *S*-ETI and *R*-ETI·$ZnCl_2$ / *S*-ETI·$ZnCl_2$ conglomerates were recorded using a Perkin-Elmer Diamond. The samples (1-3 mg range), obtained through kneading were placed in open or Al-pans. All measurements were conducted at a heating rate of 5 or 10ºC min^{-1}.

1.6 Ternary Phase Diagram. The ternary phase diagram (TPD) was constructed by slurrying *RS*-ETI and $ZnCl_2$ in ethanol, varying the molar ratio of the starting materials from 0 to 1. Experiments were carried out in a number of 2 mL sealed vials, and the suspensions were stirred at constant temperature (25 °C) over 48 h. Seeding with all possible solid-state forms was performed to make sure that the system reached thermodynamic equilibrium. Afterwards the samples were filtered by sand core funnel. The solid phases were characterized by XRPD. Concentration of zinc in the supernatant solution could not be determined via HPLC, due to transparency to UV radiation. Hence, to determine the equilibrium compositions, necessary for the determination of the solubility lines, each experimental condition described above was repeated, but this time the samples were not filtered; small portions of solvent were added to the stirring mixtures every 30 minutes, until complete dissolution of the suspended solid was observed. This allowed the construction of the solubility line in the ternary phase diagram (fig. ESI-1). TPDs were drawn with the software ProSim Ternary Diagram.

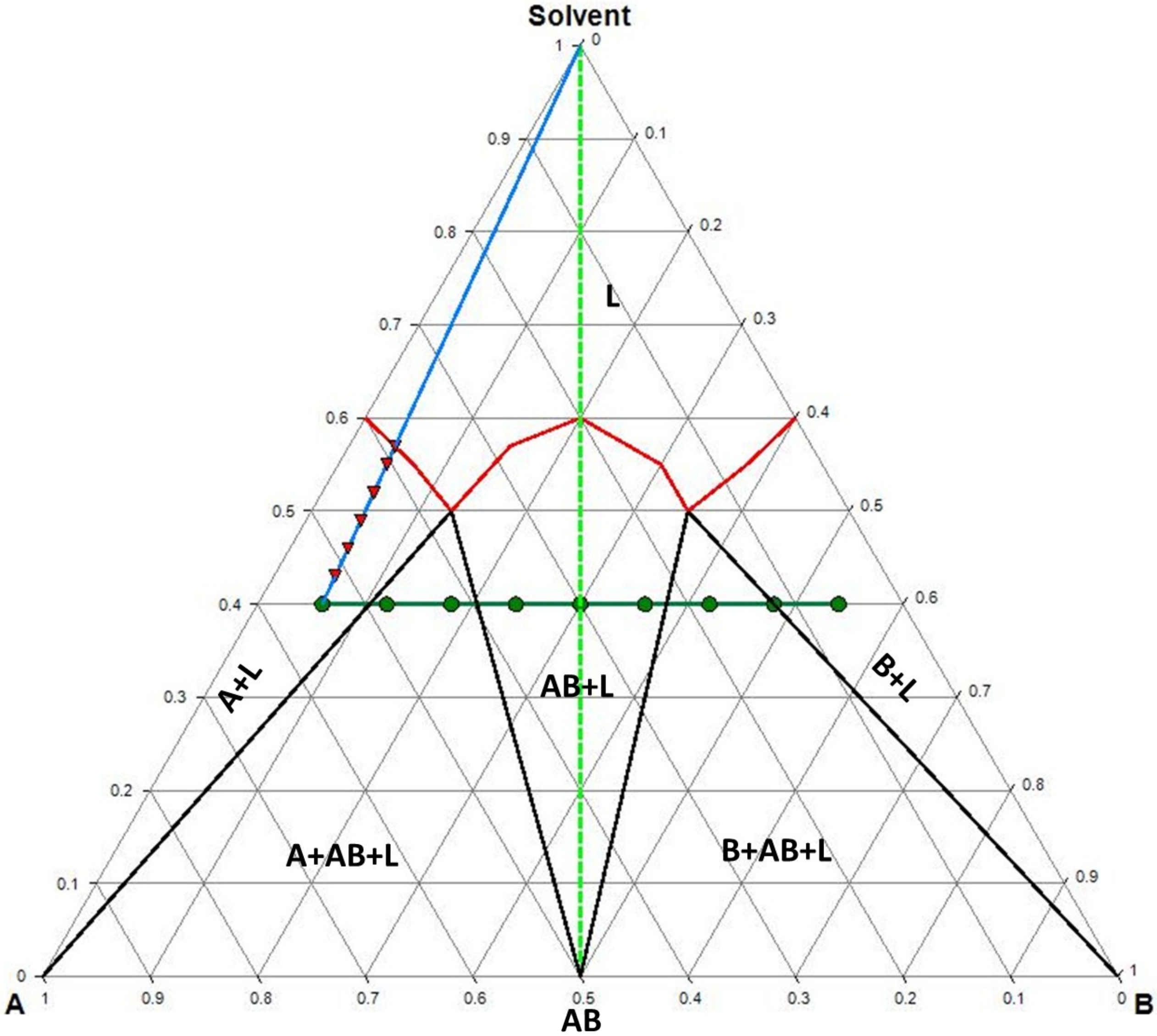

Fig. ESI-1. TPD of a generic co-crystal AB and a solvent; L is the liquid phase. Green dots: experimental ratios of the A and B components slurried in a fixed quantity of the solvent. Red broken line: solubility curve; this was determined by addition of small quantities of solvent to the known mixtures of the starting materials: in this figure the 9:1 of A:B ratio has been chosen as an example. The addition of solvent to the given suspension moves the composition towards the solvent vertex of this TPD (blue line). Each time solvent is added, one moves up a point on this line (red triangles).

2. X-ray diffraction analysis.

2.1 Single Crystal X-ray Diffraction. Single Crystal data were collected at room temperature with an Oxford Diffraction X´Calibur equipped with a graphite monochromator and a CCD detector. Mo-Kα radiation (λ = 0.71073 Å) was used. Unit cell parameters for both complexes discussed herein are reported in Table ESI-1. The structure was solved by the Intrinsic Phasing methods and refined by least squares methods again F^2 using SHELXT-2014[1] and SHELXL-2018[2] with OLEX 2 interface.[3] Non-hydrogen atoms were refined anisotropically. Hydrogen atoms were added in calculated positions and refined riding on their respective carbon or nitrogen atoms. The software Mercury 3.10.1[4] was used for graphical representations and for powder patterns simulation on the basis of single crystal data.

Table ESI-1. Crystal data and details of measurements for *S*-ETI·$ZnCl_2$ and *RS*-ETI_2·$ZnCl_2$.

	***S*-ETI·$ZnCl_2$**	***RS*-Eti_2·$ZnCl_2$**
Chemical formula	$C_{16}H_{28}Cl_4N_4O_4Zn_2$	$C_{16}H_{28}Cl_2N_4O_4Zn$
M_r, g*mol^{-1}	612.96	476.69
T / K	293 (2)	293 (2)
Morphology, colour	Block, colourless	Block, colourless
Crystal system	Monoclinic	Monoclinic
Space group	$P2_1$	*C*2/*c*
a / Å	6.3692 (3)	17.6678 (6)
b / Å	11.6771 (4)	6.9371 (2)
c / Å	17.1077 (6)	18.0628 (8)
α / °	90	90
β / °	98.496 (4)	91.515 (3)
γ / °	90	90
V / Å^3	1258.40 (9)	2213.06 (14)
Z	2	4
d / mg.cm^{-3}	1.618	1.431
μ / mm^{-1}	2.36	1.38
Measd reflns	6011	4853
Indep reflns	4612	2561
Reflns with $I > 2\sigma(I)$	4031	2118
R_{int}	0.024	0.027
$R[F^2 > 2\sigma(F^2)]$	0.0435	0.0425
$wR(F^2)$	0.092	0.098

Crystal data can be obtained free of charge from the Cambridge Crystallographic Data Centre via https://www.ccdc.cam.ac.uk and have been allocated the accession numbers **CCDC 1857803** (*RS*-ETI_2·$ZnCl_2$) and **1857804** (*S*-ETI·$ZnCl_2$).

2.2 X-ray Diffraction from Powder. For phase identification purposes X-ray powder diffraction (XRPD) patterns were collected on a PANalytical X´Pert Pro Automated diffractometer equipped with an X´celerator detector in Bragg-Brentano geometry, using Cu-Kα radiation (λ=1.5418 Å) without monochromator in 3-50° 2θ range (step size 0.033º; time/step: 20 s; Soller slit 0,04 rad, antiscatter slit: ½, divergence slit: ¼ ; 40 mA*40kV).

2.3 Variable temperature X-ray diffraction.

VT-XRPD diffractograms were collected in the 5-50° 2θ range on a PANalytical X'Pert PRO automated diffractometer, equipped with an X'Celerator detector and an Anton Paar TTK 450 system for measurements at controlled temperature. Data were collected in open air in Bragg-Brentano geometry, using Cu-Kα radiation without a monochromator. Thermal programs were selected on the basis of TGA results.

3. Experimental results

3.1 *RS*-Etiracetam and *S*-Etiracetam.

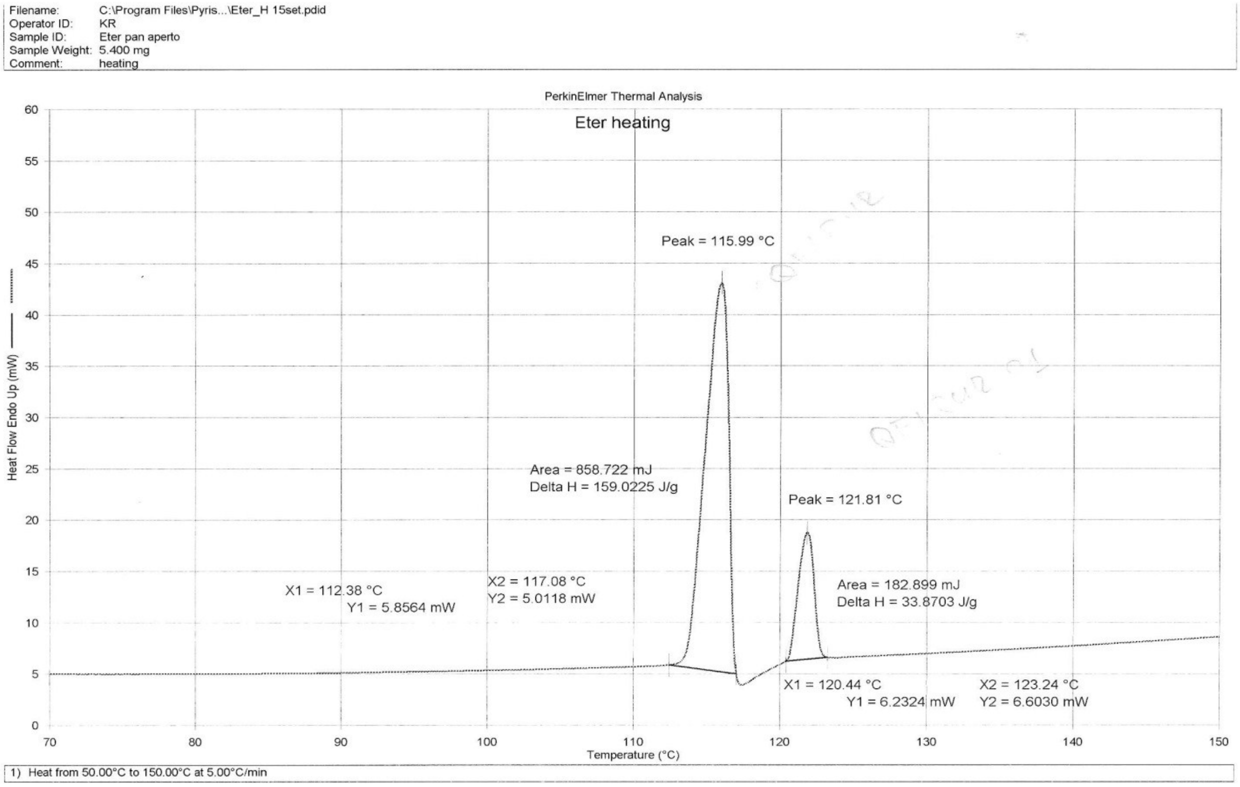

Fig. ESI-2. DSC trace for *RS*-ETI.

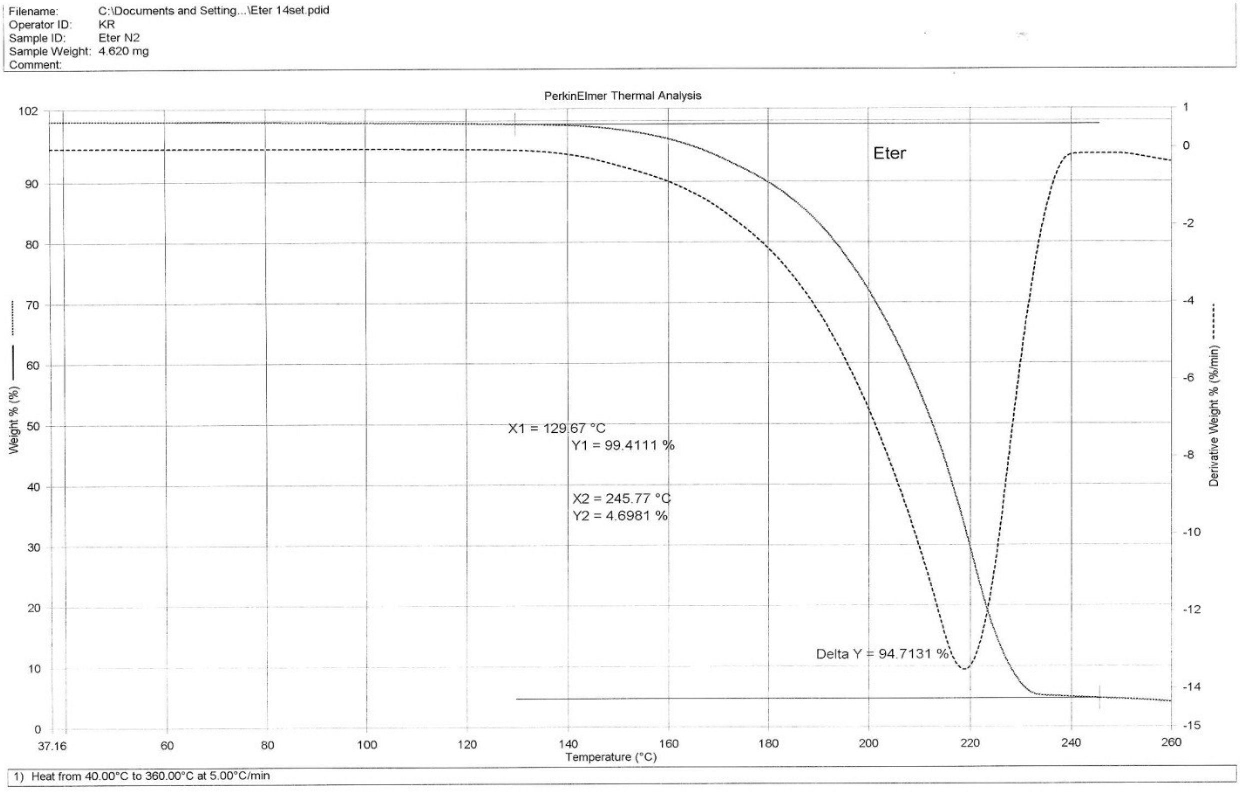

Fig. ESI-3. TGA of *RS*-ETI.

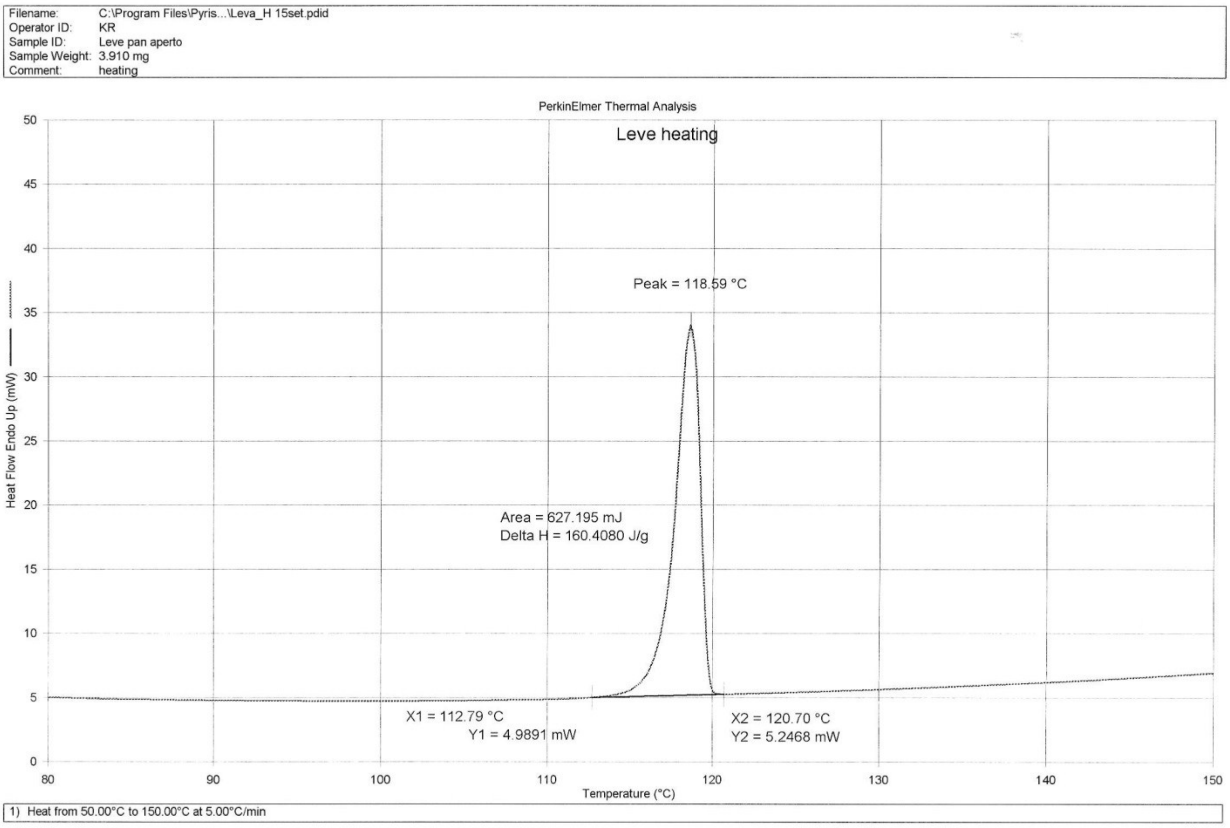

Filename: C:\Program Files\Pyris...\Leva_H 15set.pdid
Operator ID: KR
Sample ID: Leve pan aperto
Sample Weight: 3.910 mg
Comment: heating

1) Heat from 50.00°C to 150.00°C at 5.00°C/min

Fig. ESI-3. DSC trace for *S*-ETI.

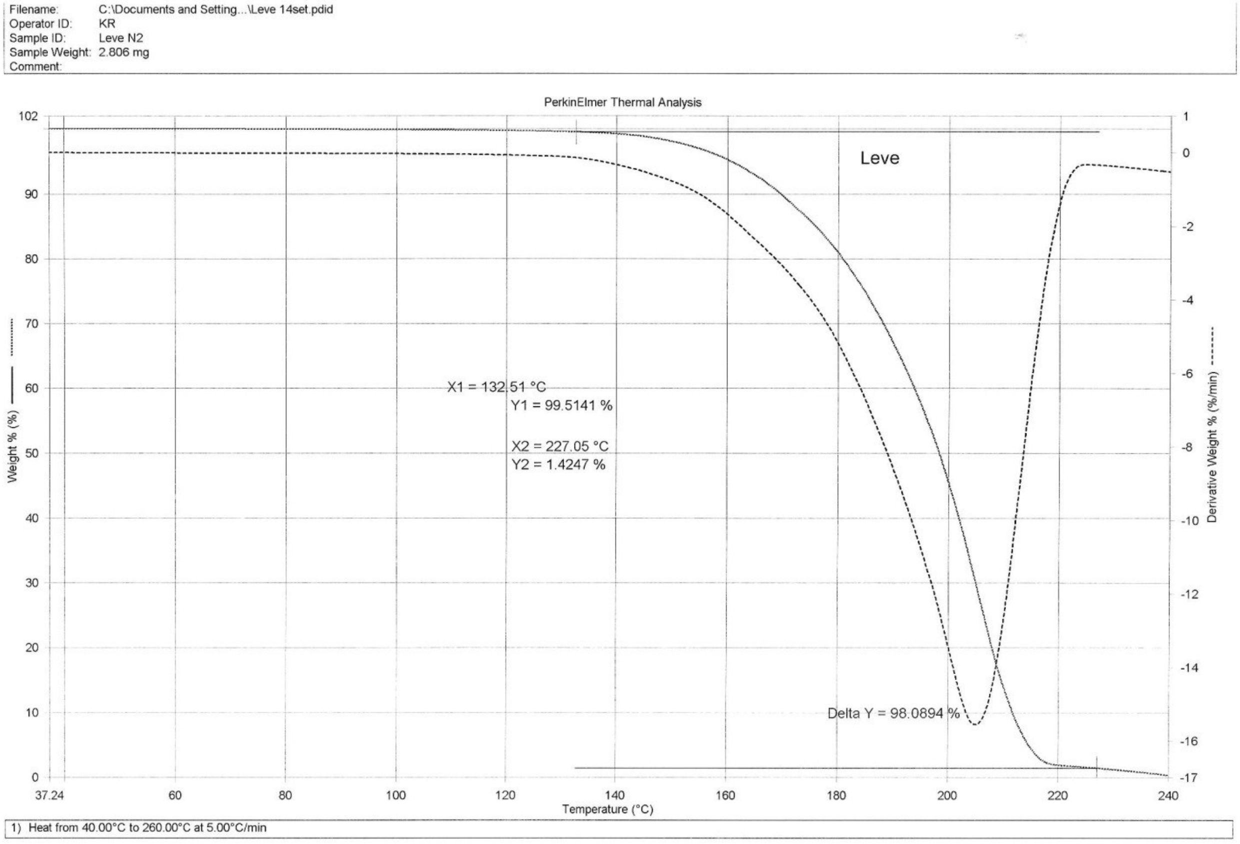

Filename: C:\Documents and Setting...\Leve 14set.pdid
Operator ID: KR
Sample ID: Leve N2
Sample Weight: 2.806 mg
Comment:

1) Heat from 40.00°C to 260.00°C at 5.00°C/min

Fig. ESI-4. DSC thermogram of *S*-ETI.

3.2 ***RS*-ETI$_2$·ZnCl$_2$**

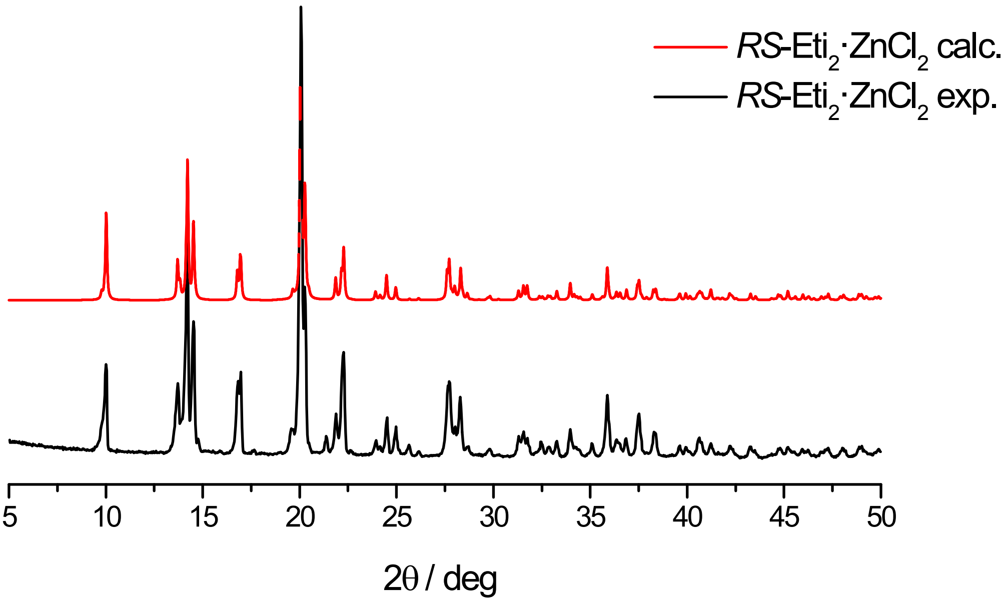

Fig. ESI-5. Comparison between the experimental (crystallization from solution) and calculated XRPD patterns for *RS*-ETI$_2$·ZnCl$_2$.

The TGA shows a degradation process starting at 200°C, with DSC showing a single melting process at 132°C (onset), ca. 40°C lower than the one observed for *S*-ETI·ZnCl$_2$ (see below). VT-XRPD confirms (i) the presence of only one form and (ii) the melting of that form at higher temperatures. Recrystallization from the melt is not observed.

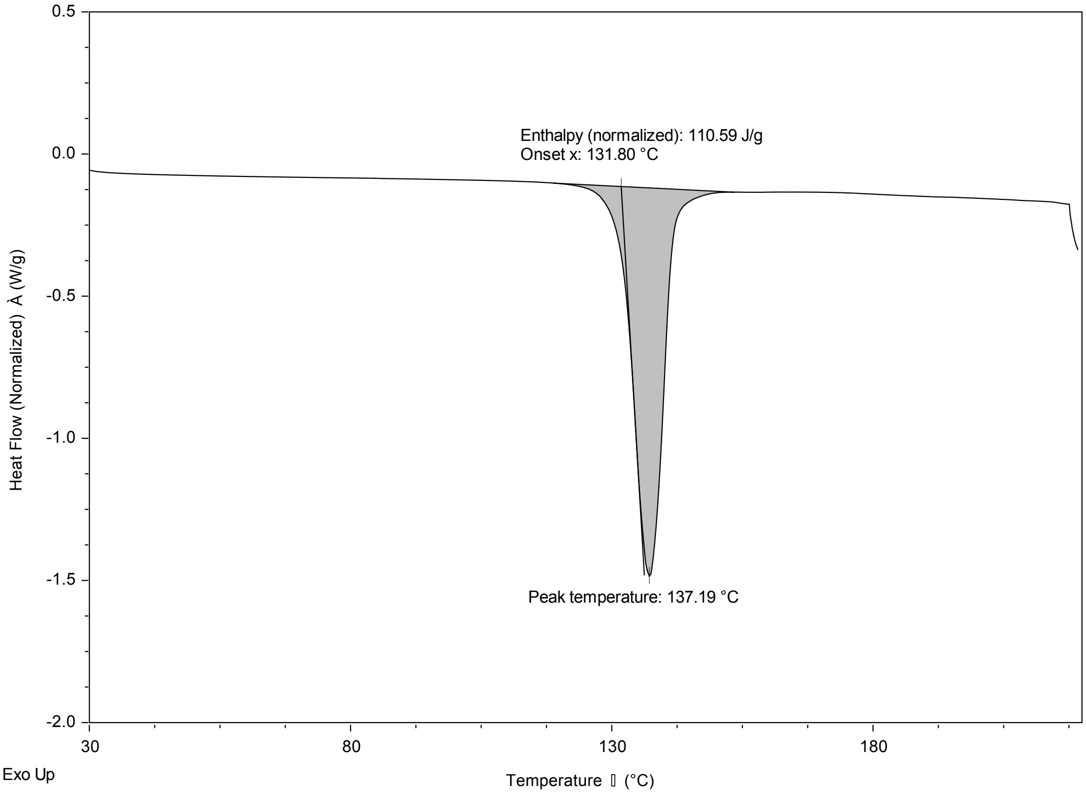

Fig. ESI-6. DSC trace of *RS*-ETI$_2$·ZnCl$_2$.

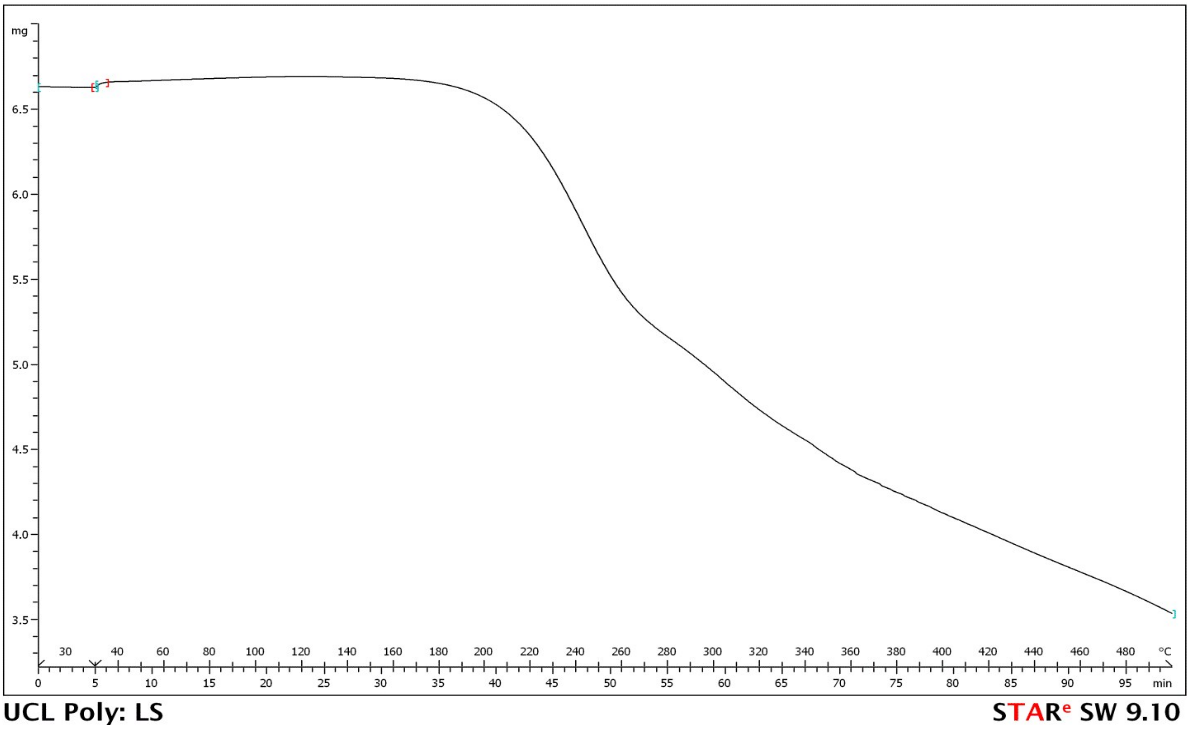

Fig. ESI-7.: TGA of *RS*-ETI$_2$·ZnCl$_2$.

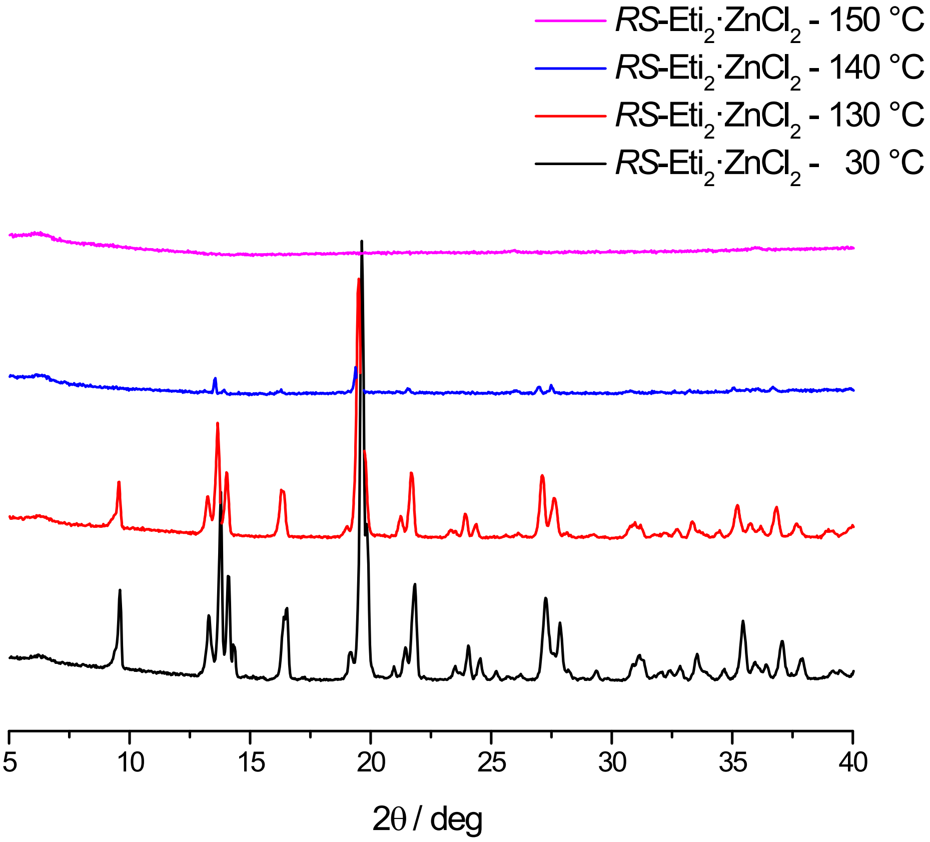

Fig. ESI-8.: VT-XRPD for *RS*-ETI$_2$·ZnCl$_2$.

3.3 *S*-ETI·ZnCl$_2$

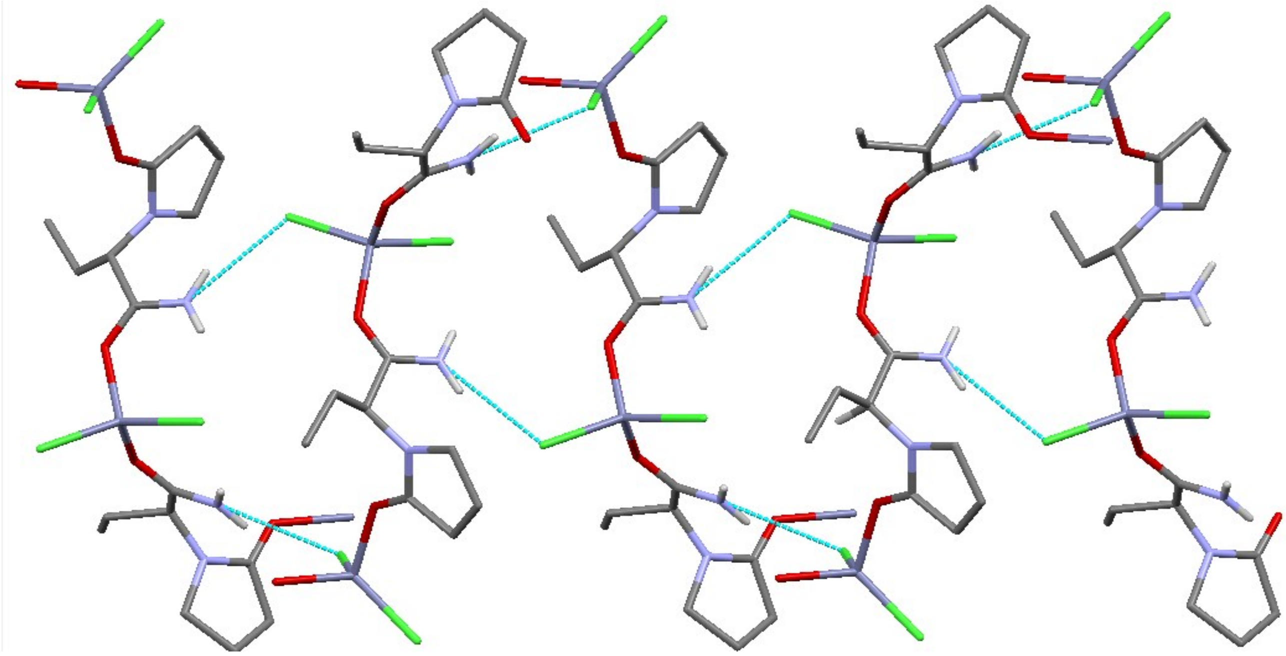

Fig. ESI-9.: *S*-ETI·ZnCl$_2$. Hydrogen bonds between the chloride anions and the hydrogen atoms of the amido groups that hold together the zig-zag chains formed by ZnCl$_2$ units bridged by *S*-etiracetam molecules.

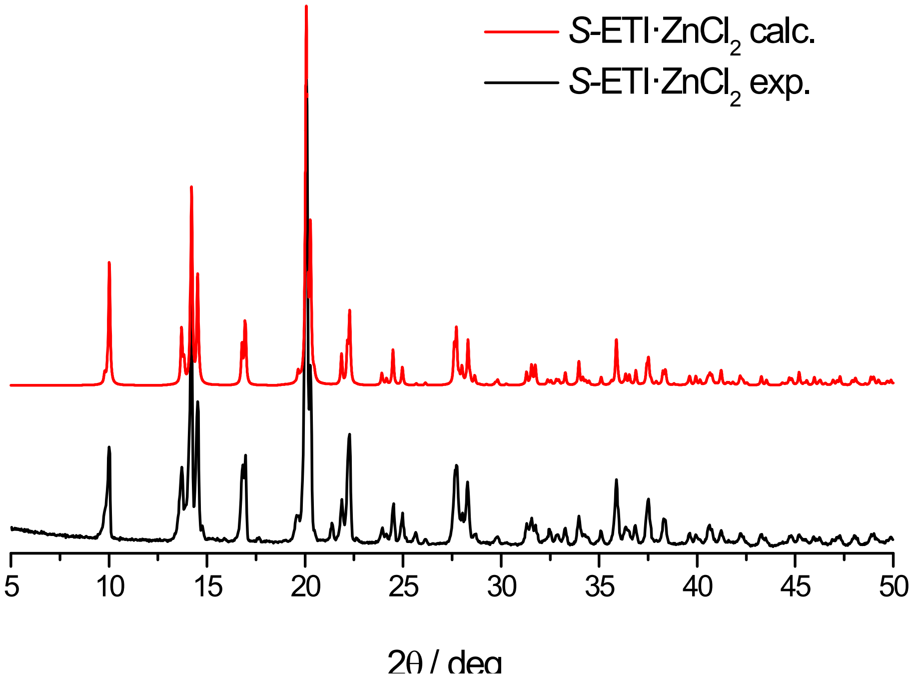

Fig. ESI-10. Comparison between the experimental (crystallization from solution) and calculated XRPD patterns for *S*-ETI·ZnCl$_2$.

The TGA trace shows a degradation process starting at 220°C. A small initial mass loss is likely due to removal of residual solvent adsorbed on the surface of the sample. A similar observation can be made on the basis of the DSC trace, which shows an initial endotherm, which can easily be attributed to evaporation of residual solvent; at 176°C (onset) melting is observed. VT-XRPD confirms that only one form is present and melting of that form occurs above 180°C. Recrystallization from the melt is not observed.

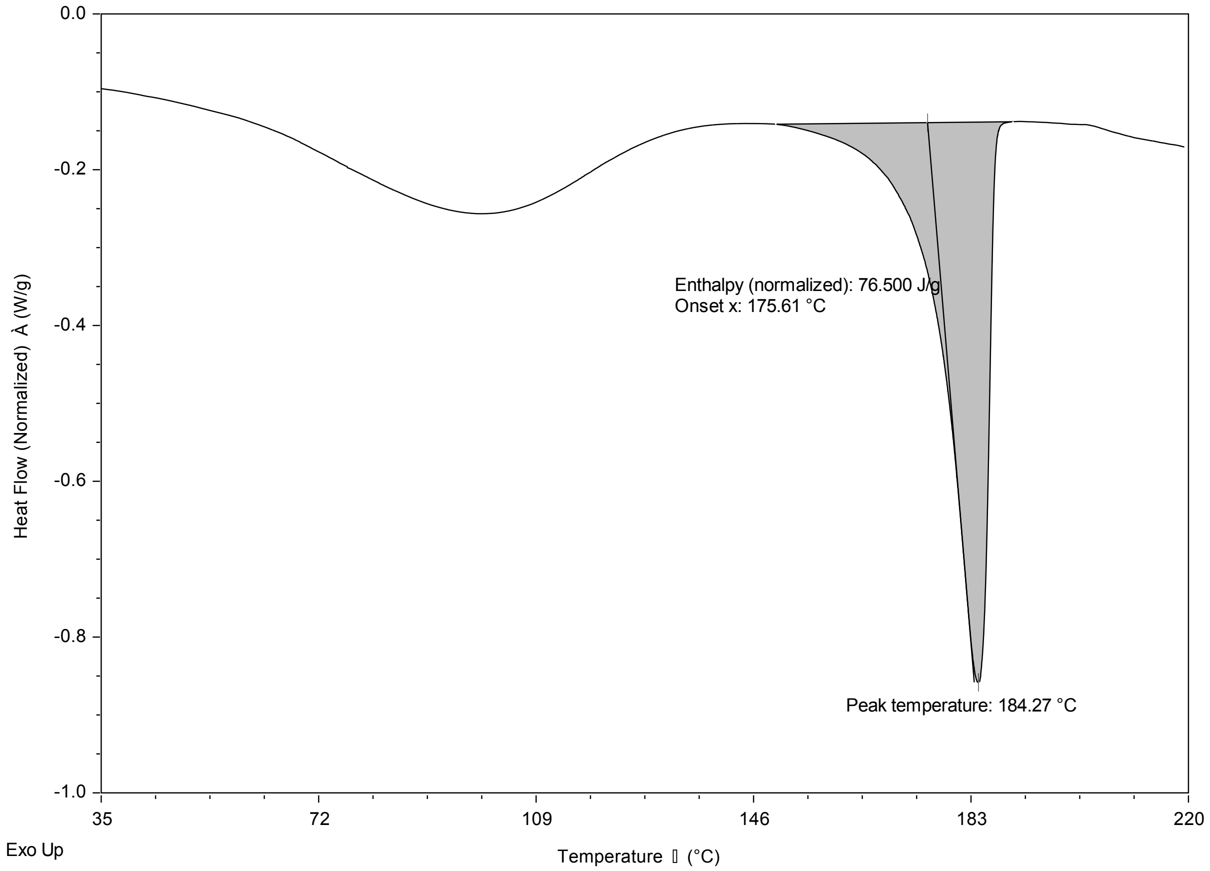

Fig. ESI-11. DSC thermogram of *S*-ETI·$ZnCl_2$.

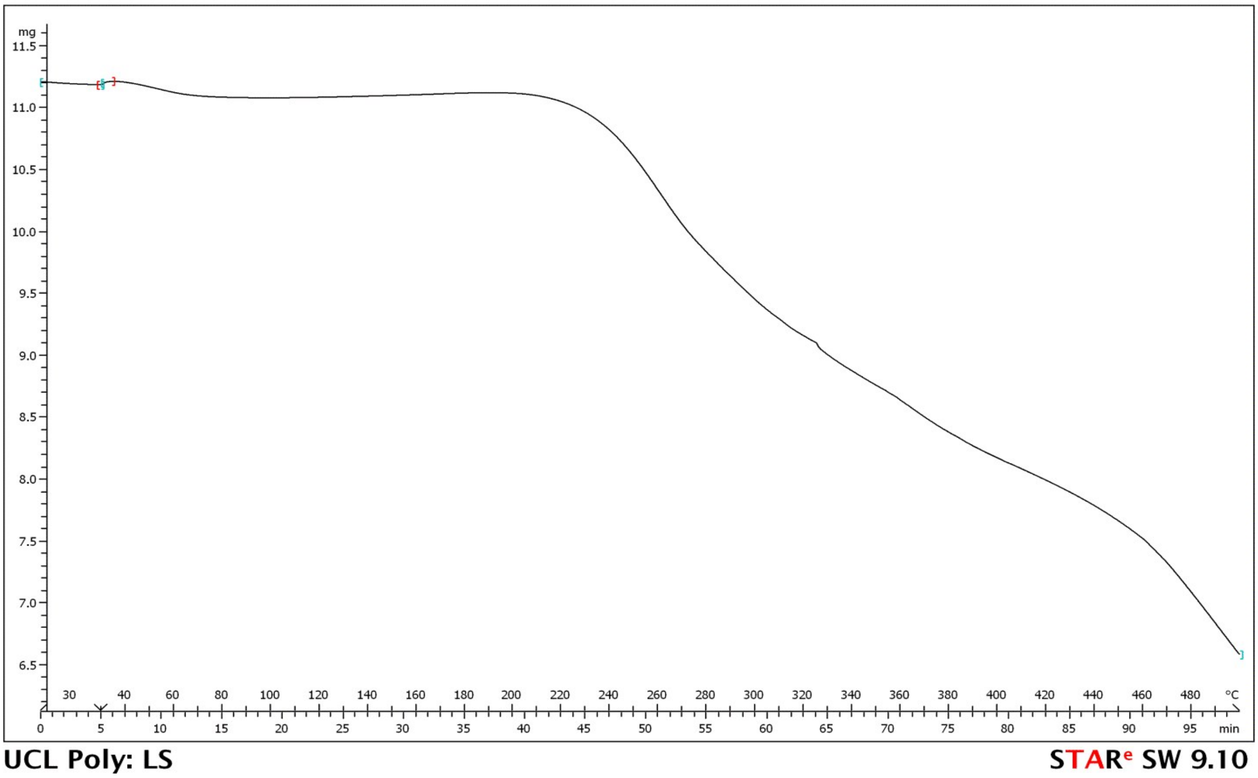

Fig. ESI-12. TGA analysis of *S*-ETI·$ZnCl_2$.

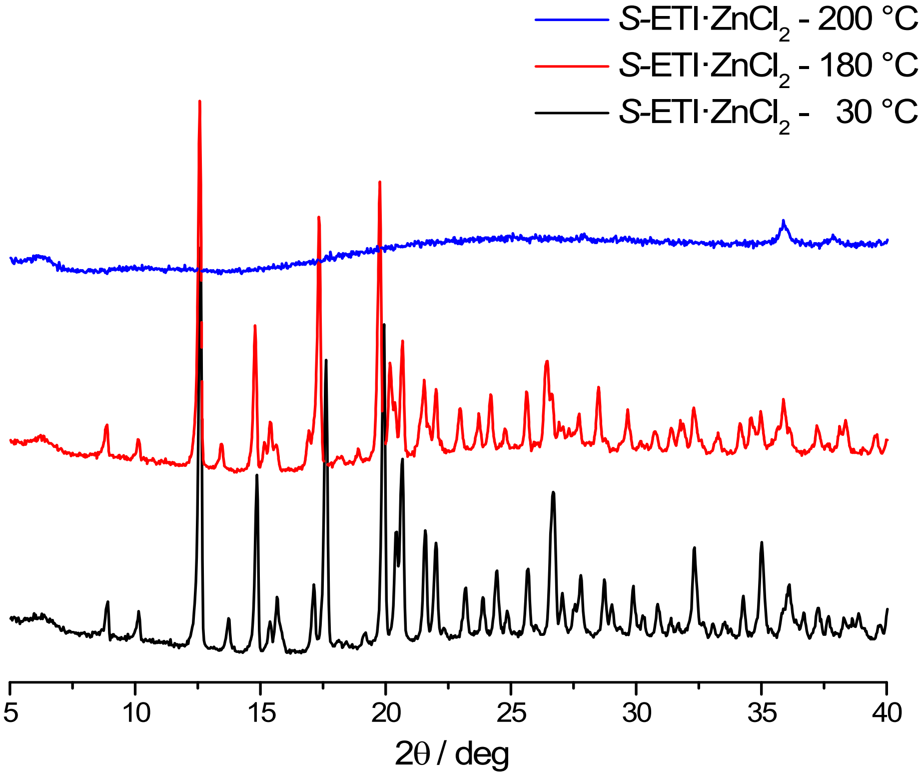

Fig. ESI-13. VT-XRPD for *S*-ETI·$ZnCl_2$.

3.4 *R*-ETI·ZnCl₂ / *S*-ETI·ZnCl₂ conglomerate

DSC analysis shows a single endothermic event, attributable to melting, at 156.64°C (onset), that is approximately 20 ° lower than the 176°C observed for the single enantiomer (Fig. ESI-11), as it can be expected for a conglomerate.[5]

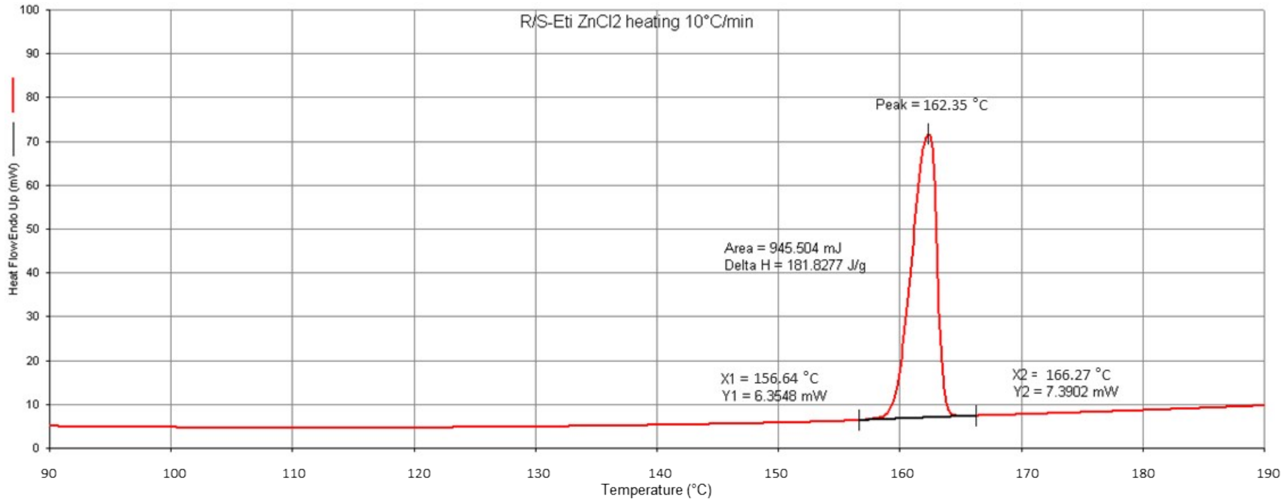

Fig. ESI-14. DSC trace for the *R*-ETI·$ZnCl_2$ / *S*-ETI·$ZnCl_2$ conglomerates.

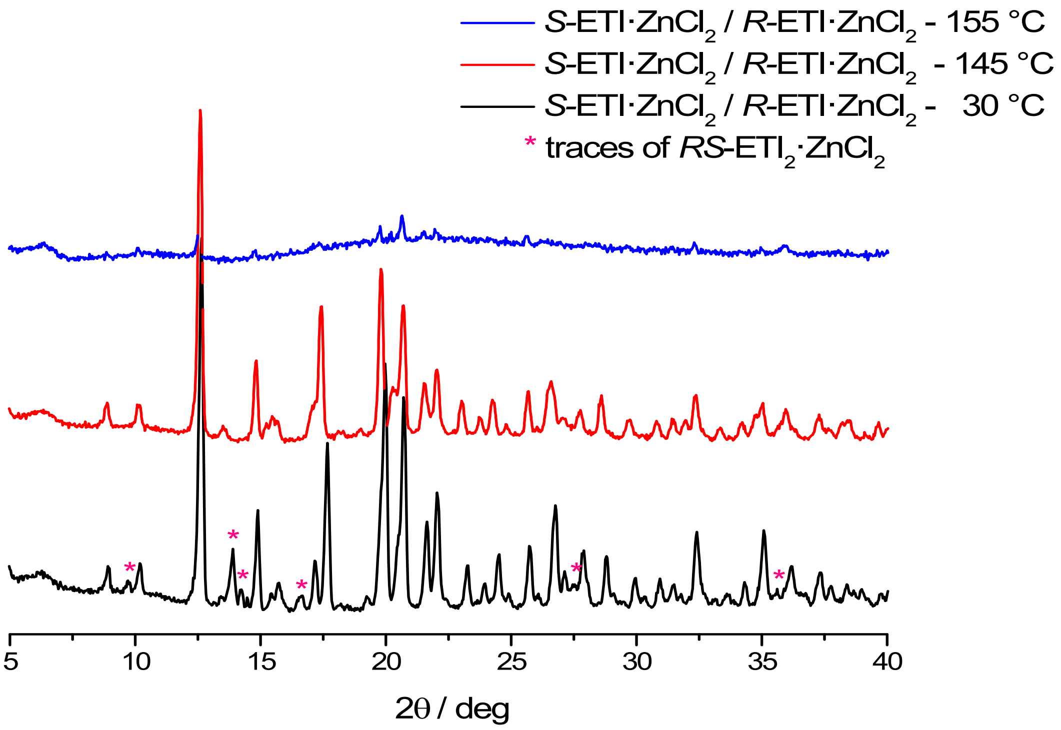

Fig. ESI-15. VT-XRPD for the *R*-ETI·$ZnCl_2$ / *S*-ETI·$ZnCl_2$ conglomerate. Some traces of *RS*-ETI_2·$ZnCl_2$ are present in the sample (the corresponding peaks are marked with asterisks). Upon reaching 145 °C the peaks of the racemic complex are not observed any longer in the diffractograms, whereas the conglomerates are still stable.

4. TPD for the *RS*-ETI:$ZnCl_2$:ethanol system.

To construct a TPD for the *RS*-ETI:$ZnCl_2$ system a series of physical mixtures of starting materials (200 mg of total weight) were prepared (see table ESI-2). To the obtained mixtures 0.35 mL of ethanol were added and slurry experiments performed at 25°C for 48h. The samples with the suspensions were seeded with both starting materials and with RS-$ETI_2 \cdot ZnCl_2$. Seeding material was prepared by kneading with ethanol (see synthesis).

Table ESI-2. Initial Experimental Data for System of *RS*-ETI:$ZnCl_2$:EtOH at 298 K. 200 mg of total weight of *RS*-ETI:$ZnCl_2$ in 0.35mL of EtOH.

Initial composition *RS*-ETI:$ZnCl_2$ (%)	**Initial components**			**Initial components (mol %)**			**Solid phase at equilibrium**
	***RS*-ETI (mg)**	**$ZnCl_2$ (mg)**	**EtOH (ml)**	***RS*-ETI**	**$ZnCl_2$**	**EtOH**	
90:10	182.52	17.48	**0.35**	0.117	0.013	0.870	*RS*-ETI+ *RS*-$ETI_2 \cdot ZnCl_2$
80:20	164.55	35.45	0.35	0.105	0.026	0.868	*RS*-ETI+ *RS*-$ETI_2 \cdot ZnCl_2$
70:30	146.06	53.94	0.35	0.093	0.040	0.867	*RS*-$ETI_2 \cdot ZnCl_2$
60:40	127.03	72.97	0.35	0.081	0.054	0.865	*RS*-$ETI_2 \cdot ZnCl_2$
50:50	107.43	92.57	0.35	0.068	0.068	0.863	*RS*-$ETI_2 \cdot ZnCl_2$
40:60	87.24	112.76	0.35	0.055	0.083	0.861	*RS*-$ETI_2 \cdot ZnCl_2$ + *R*-$ETI \cdot ZnCl_2$/*S*-$ETI \cdot ZnCl_2$
30:70	66.43	133.57	0.35	0.042	0.098	0.860	Dissolved
20:80	44.98	155.02	0.35	0.028	0.114	0.858	Dissolved
10:90	22.84	177.16	0.35	0.014	0.130	0.856	Dissolved

Taking into account the fact that the given quantity of starting materials completely dissolved in all the cases where the excess of $ZnCl_2$ was employed, the experiment was repeated using 500 mg of total weight and 0.3 mL of EtOH (see table ESI-3).

Table ESI-3. Initial Experimental Data for System of *RS*-ETI:$ZnCl_2$:EtOH at 298 K. 500 mg of total weight of *RS*-ETI:$ZnCl_2$ in 0.3mL of EtOH.

Initial composition *RS*-ETI:$ZnCl_2$ (%)	**Initial components**			**Initial components (mol %)**			**Solid phase at equilibrium**
	***RS*-ETI (mg)**	**$ZnCl_2$ (mg)**	**EtOH (mL)**	***RS*-ETI**	**$ZnCl_2$**	**EtOH**	
90:10	456.31	43.69	**0.3**	0.314	0.035	0.652	*RS*-ETI_2·$ZnCl_2$ + *RS*-ETI
80:20	411.38	88.62	0.3	0.281	0.07	0.648	*RS*-ETI_2·$ZnCl_2$ + *RS*-ETI
70:30	365.15	134.85	0.3	0.248	0.106	0.645	*RS*-ETI_2·$ZnCl_2$ + *RS*-ETI
60:40	317.56	182.44	0.3	0.215	0.143	0.642	*RS*-ETI_2·$ZnCl_2$ + *R*-ETI·$ZnCl_2$/*S*-ETI·$ZnCl_2$
50:50	268.57	231.43	0.3	0.181	0.181	0.638	*RS*-ETI_2·$ZnCl_2$ + *R*-ETI·$ZnCl_2$/*S*-ETI·$ZnCl_2$
40:60	218.09	281.91	0.3	0.146	0.219	0.635	*R*-ETI·$ZnCl_2$/*S*-ETI·$ZnCl_2$
30:70	166.07	333.93	0.3	0.111	0.258	0.631	*R*-ETI·$ZnCl_2$/*S*-ETI·$ZnCl_2$
20:80	112.44	387.56	0.3	0.074	0.298	0.628	*R*-ETI·$ZnCl_2$/*S*-ETI·$ZnCl_2$
10:90	57.11	442.89	0.3	0.038	0.338	0.624	Too little quantity of material to perform XRPD analysis

The solubility curve was determined by adding small portions of ethanol to the stirring mixtures every 30 minutes, until the suspended solids were completely dissolved (see table ESI-4).

Table ESI-4. Experimental Data for the Dissolution Points at 298 K

Initial composition *RS*-ETI:ZnCl$_2$ (%)	**EtOH initial (ml)**	**EtOH added (ml)**	**Composition at dissolution point**			**Composition at dissolution point (mol %)**		
			***RS*-ETI (mg)**	**ZnCl$_2$ (mg)**	**EtOH (mL)**	***RS*-ETI**	**ZnCl$_2$**	**EtOH**
100:0	**0.3**	**3.95**	**500.00**	**0**	**4.25**	0.042	0.000	0.958
90:10	0.3	**2.95**	456.31	43.69	**3.25**	0.049	0.005	0.946
80:20	0.3	**3.55**	411.38	88.62	**3.85**	0.038	0.009	0.953
70:30	0.3	**3.75**	365.15	134.85	**4.05**	0.032	0.014	0.955
60:40	0.3	**3.95**	317.56	182.44	**4.25**	0.026	0.018	0.956
50:50	0.3	**2.3**	268.57	231.43	**2.6**	0.035	0.035	0.929
40:60	0.3	**1.2**	218.09	281.91	**1.5**	0.047	0.071	0.882
30:70	0.3	**0.7**	166.07	333.93	**1.0**	0.051	0.119	0.830
20:80	0.3	**0.5**	112.44	387.56	**0.8**	0.059	0.235	0.707
10:90	0.3	**0.1**	57.11	442.89	**0.4**	0.035	0.311	0.655
0:100	0.3	**0.2**	**0**	**500.00**	**0.5**	0.000	0.300	0.700

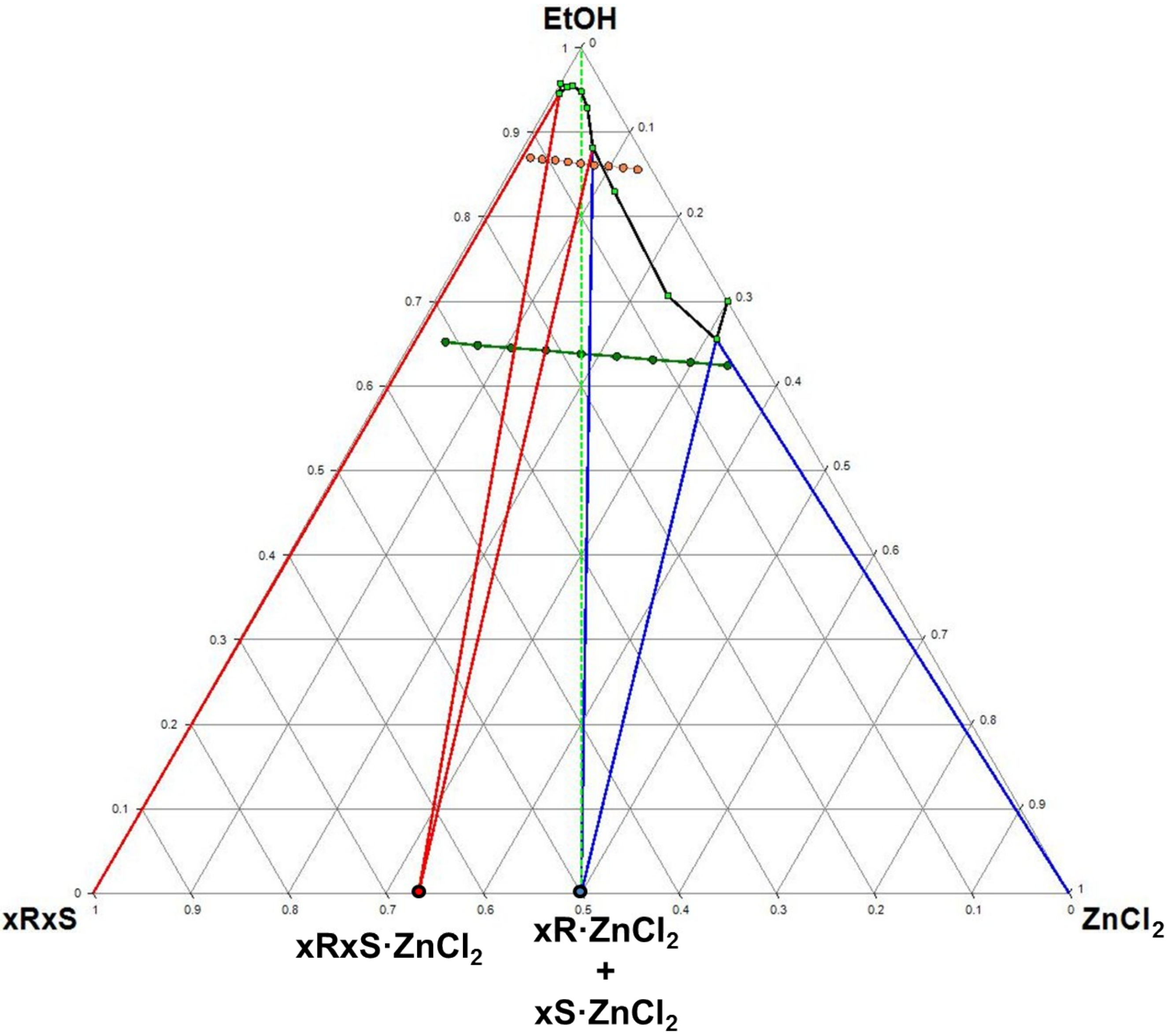

Fig. ESI-16. Complete ternary phase diagram for *RS*-ETI:ZnCl$_2$:EtOH at 298K (mol%). RS corresponds to R- and S-etiracetam correspondingly. **x** corresponds to the molecular ratio of R- and S-etiracetam.

References

1. G. M. Sheldrick, *Acta Crystallographica Section A Foundations and Advances*, 2015, **71**, 3-8.
2. G. M. Sheldrick, *Acta Crystallographica Section C Structural Chemistry*, 2015, **71**, 3-8.
3. O. V. Dolomanov, L. J. Bourhis, R. J. Gildea, J. A. K. Howard and H. Puschmann, *J. Appl. Crystallogr.*, 2009, **42**, 339-341.
4. C. F. Macrae, P. R. Edgington, P. McCabe, E. Pidcock, G. P. Shields, R. Taylor, M. Towler and J. van De Streek, *Journal of Applied Crystallography*, 2006, **39**, 453-457.
5. H. G. Brittain in *Polymorphism in Pharmaceutical Solids*, *Vol. 162* Informa Healthcare USA, Inc., **2009**.